1999

Analysis of a Lithium/Thionyl Chloride Battery under Moderate-Rate Discharge

Mukul Jain
University of South Carolina - Columbia

Ganesan Nagasubramanian

Rudolph G. Jungst

John W. Weidner
University of South Carolina - Columbia, weidner@engr.sc.edu

Publication Info

Journal of the Electrochemical Society, 1999, pages 4023-4030.

Journal of The Electrochemical Society, **146** (11) 4023-4030 (1999)
S0013-4651(98)07-107-9 CCC: $7.00 © The Electrochemical Society, Inc.

Analysis of a Lithium/Thionyl Chloride Battery under Moderate-Rate Discharge

Mukul Jain,[a,*,c] Ganesan Nagasubramanian,[b,*] Rudolph G. Jungst,[b,*] and John W. Weidner[a,*]

[a]*Center for Electrochemical Engineering, Department of Chemical Engineering, University of South Carolina, Columbia, South Carolina 29208, USA*
[b]*Sandia National Laboratories, Albuquerque, New Mexico 87185, USA*

A one-dimensional mathematical model of a spirally wound lithium/thionyl chloride primary battery is developed and used for parameter estimation and design studies. The model formulation is based on the fundamental conservation laws using porous electrode theory and concentrated solution theory. The model is used to estimate the transference number, the diffusion coefficient, and the kinetic parameters for the reactions at the anode and the cathode as a function of temperature. These parameters are obtained by fitting the simulated capacity and average cell voltage to experimental data over a wide range of temperatures (−55 to 49°C) and discharge loads (10-250 Ω). The experiments were performed on D-sized, cathode-limited, spirally wound lithium/thionyl chloride cells. The model is also used to study the effect of cathode thickness on the cell capacity as a function of temperature, and it was found that the optimum thickness for the cathode-limited design is temperature and load dependent.

Manuscript submitted July 30, 1998; revised manuscript received July 9, 1999.

The lithium/thionyl chloride battery ($Li/SOCl_2$) has received considerable attention as a primary energy source due to its high energy density, high operating cell voltage, voltage stability over 95% of the discharge, large operating temperature range (−55 to 70°C), long storage life, and low cost of materials.[1,2] However, a loss in performance may occur after periods of prolonged storage at high and low temperatures or when exposed to intermittent use. This loss in performance may result in reduced capacity or even worse, catastrophic failure, especially when operated at high discharge rates. High discharge rates and high temperatures promote thermal runaway, which can result in the venting of toxic gases and explosion.[2]

Mathematical models can be used to tailor a battery design to a specific application, perform accelerated testing, and reduce the amount of experimental data required to yield efficient, yet safe cells. Models can also be used in conjunction with the experimental data for parameter estimation and to obtain insights into the fundamental processes occurring in the battery. Previous investigators[3,4] presented a one-dimensional mathematical model of the $Li/SOCl_2$ battery. They used porous electrode theory[5] to model the porous cathode and concentrated solution theory[6] for the electrolyte solution to study the effect of various design and operational parameters on the discharge curves. The model equations were written under the assumption that the excess electrolyte was in a reservoir between the separator and the porous cathode. The result was that the electrolyte replenished the porous cathode through the front face of the electrode. The theoretical results showed similar qualitative trends to those observed experimentally. However, a lack of experimental data and unknown values for many of the kinetic and transport parameters as a function of temperature prevented quantitative comparisons. Evans and White[7] presented a parameter estimation technique and used it in conjunction with the one-dimensional mathematical model presented earlier.[4] However, the comparison between simulated and experimental discharge curves was done only for partially discharged cells at ambient temperature.

This paper presents a one-dimensional mathematical model for the $Li/SOCl_2$ cell, with model equations similar to those presented previously.[3,4] The exception is the modification to the material balance in the porous cathode that accounts for electrolyte replenishment through the top rather than the front of the porous cathode.[8] The model is used to predict discharge curves at low-to-moderate discharge rates (discharge loads ≤10 Ω, corresponding to current densities less than 2 mA/cm^2 for a D-size cell). Previous thermal models of $Li/SOCl_2$ cells have shown that under these operating conditions thermal runaway is not a problem.[9,10] Therefore, it is also assumed here that the temperature of the cell is uniform throughout but allowed to change during discharge.[3,4]

The model is then used in conjunction with experimental data to obtain estimates for the transference number, diffusion coefficient, and kinetic parameters for the reactions at the anode and cathode as a function of temperature. Using the estimated parameters, the model predictions show good agreement with the experimental data over a wide temperature (−55 to 49°C) and load range (10 to 250 Ω). Finally, the model is used to study the effect of cathode thickness on cell performance as a function of operating temperature and load to illustrate the application in optimization studies.

Experimental

The D-size spirally wound $Li-SOCl_2$ cells used in the experiments were obtained from Eagle Pitcher Technologies. The cells consisted of a carbon cathode, lithium anode, and two Whatman DBS45-1 borosilicate glass separators. The assembly is rolled together (anode, separator, cathode, and then separator), and the roll is inserted into a stainless steel cell can with a prewelded burst disk in the base. The cell can is equipped with a stainless steel header assembly with prewelded nickel tabs for the Li anode. The cells were filled in an inert atmosphere of argon with 28 mL of electrolyte consisting of 1.0 M $LiAlCl_4$ in $SOCl_2$.

The cells were discharged at different loads ranging from 10 to 250 Ω using a model BT2042 Arbin battery cycler. The discharge measurements were carried out in a controlled temperature environment to study the effect of temperature, and the temperature during tests was controlled with a benchtop model Tenney Jr. temperature chamber. A cutoff voltage of 2.0 V was used to note the capacity delivered by the cell for a constant load discharge at a given temperature. Multiple experiments were conducted for the same conditions, and the data reported in this work are an average of three or more experiments.

Model Development

Figure 1 shows a schematic of the one-dimensional cell as modeled in this work. This schematic shows the cross section of a spirally wound $Li/SOCl_2$ cell. The four regions in the schematic are the lithium foil anode, the lithium chloride (LiCl) film that forms on the anode surface, the separator (usually glass matting), and the porous carbon cathode. The electrolyte consists of 1.0 M lithium tetrachloroaluminate ($LiAlCl_4$) in thionyl chloride ($SOCl_2$). The components are rolled together and inserted in a cylindrical can (commer-

* Electrochemical Society Active Member.
[c] Present address: Medtronic, Incorporated, Minneapolis, Minnesota 55430, USA.

S0013-4651(98)07-107-9 CCC: $7.00

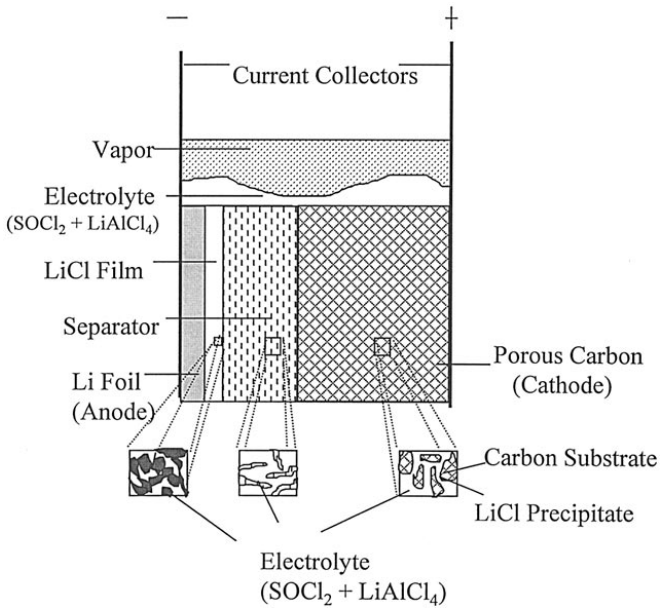

Figure 1. Schematic of a Li/$SOCl_2$ cell. The anode, separator, and the porous cathode are stacked together, and the assembly is spirally wound and inserted in a D-size cell can.

cial D-size). Electrolyte is then poured into the can, filling the porous regions of the roll, and the excess electrolyte resides at the top of the electrode/separator assembly. The anode surface and the cathode current collector are the boundaries of the model region. The overall reactions included in the model are the oxidation of lithium at the anode

$$\mathrm{Li} \rightarrow \mathrm{Li}^+ + \mathrm{e}^- \qquad [1]$$

and the reduction of $SOCl_2$ followed by precipitation of LiCl at the cathode

$$4\mathrm{Li}^+ + 4\mathrm{e}^- + 2\mathrm{SOCl}_2 \rightarrow 4\mathrm{LiCl} + \mathrm{SO}_2 + \mathrm{S} \qquad [2]$$

The $SOCl_2$ is the solvent, and $LiAlCl_4$ is the electrolyte salt.

The mathematical model developed here is similar to that developed by previous investigators.[3,4] The exception is the modification to the material balance in the porous cathode that accounts for electrolyte replenishment through the top rather than the front of the porous cathode.[8] Therefore, only the governing equations in the porous cathode are shown here, while the assumptions and other model equations can be found elsewhere.[3,4] The equations presented here also serve to place the physical parameters that are extracted from the data in a convenient context.

Porous cathode.—Conservation of mass and current, species transport, and reaction kinetics in the porous cathode are used to formulate the governing equations for the Li/$SOCl_2$ cell. Macroscopic theory of porous electrodes[5,6] is employed, where the porous region is considered to be a superposition of two continua, the electrolyte (ionically conducting solution phase) and the matrix (electronically conducting solid phase). The dependent variables are averaged over a differential volume of this two-phase continuum. These averaged quantities are continuous in time and space, and the differential volume element is large compared to the pore dimensions, yet small relative to the electrode dimensions.

Electroneutrality and conservation of mass for completely dissociated $LiAlCl_4$ salt gives

$$c = c_+ = c_- \qquad [3]$$

By conservation of charge, the charge leaving the matrix phase must equal the charge entering the solution phase. This can be expressed mathematically as

$$j_2 = \frac{\partial i_\mathrm{e}}{\partial x} = -\frac{\partial i_\mathrm{m}}{\partial x} \qquad [4]$$

where j_2 is the rate of electrochemical reaction per unit volume of the cathode for $SOCl_2$ reduction (*i.e.*, reaction 2).

The polarization relationship for $SOCl_2$ reduction in the porous cathode is represented by the following modified Butler-Volmer expression in a manner similar to previous models[3,4]

$$j_2 = a i_{\mathrm{o},2,\mathrm{ref}} \left[\exp\left(\frac{\alpha_{\mathrm{a},2} F}{RT} \eta_2 \right) - \left(\frac{c}{c_\mathrm{ref}} \right)^2 \left(\frac{c_\mathrm{o}}{c_{\mathrm{o,ref}}} \right) \exp\left(-\frac{\alpha_{\mathrm{c},2} F}{RT} \eta_2 \right) \right] \qquad [5]$$

where the overpotential is given by

$$\eta_2 = \phi_\mathrm{m} - \phi_\mathrm{e} - U_{2,\mathrm{ref}} \qquad [6]$$

The available active surface area per unit volume changes due to LiCl precipitation and is expressed as

$$a = a^\mathrm{o} \left[1 - \left(\frac{\epsilon^\mathrm{o} - \epsilon}{\epsilon^\mathrm{o}} \right)^\xi \right] \qquad [7]$$

where ξ is an experimentally determined parameter used to describe the morphology of the precipitate. Large values of ξ indicate needle-shaped deposits whereas small values represent flat deposits.[12]

The material balances for the salt and the solvent given previously[3,4] have to be modified to account for the flux of electrolyte from the header space directly into the cathode.[8] The material balance for the electrolyte salt is given by

$$\epsilon \frac{\partial c}{\partial t} + c \frac{\partial \epsilon}{\partial t} = -\frac{\partial}{\partial x} \left(-D\epsilon^{1.5} \frac{\partial c}{\partial x} + \frac{i_\mathrm{e} t_+^\bullet}{F} + c v^\bullet \right) + \frac{j_2}{F} \left[1 - \frac{c^\mathrm{o}}{2} (\hat{V}_\mathrm{o} - 2\hat{V}_\mathrm{LiCl}) \right] \qquad [8]$$

and a similar material balance can be written for the solvent. Since the porosity in the cathode changes with time due to precipitation of LiCl, a solid phase balance is required for the porous cathode. The rate of change of cathode porosity can be related to the rate of reaction, given as

$$\frac{\partial \epsilon}{\partial t} = \frac{\hat{V}_\mathrm{LiCl}}{F} j_2 \qquad [9]$$

The precipitation of LiCl also results in an expansion of the cathode, known as cathode swelling. The effect of cathode swelling on the dimensions of the cathode are treated here by modifying the cathode's matrix-phase thickness and porosity, as explained later in the parameter estimation section.

The relationship between the partial molar volumes is used to eliminate the solvent concentration, c_o. The partial volumes of electrolyte salt and the solvent add to one in each region, and this relationship can be expressed as

$$c\hat{V} + c_\mathrm{o}\hat{V}_\mathrm{o} = 1 \qquad [10]$$

where $\hat{V}$ is the partial molar volume of the electrolyte salt, $LiAlCl_4$. The solvent balance along with Eq. 8-10 can be combined to yield the following expression for the mass-average velocity

$$v^\bullet = \frac{i_\mathrm{e} \hat{V} t_-^\bullet}{F} \qquad [11]$$

The solution current is due to the movement of ions, which for this system can be expressed as

S0013-4651(98)07-107-9 CCC: $7.00

$$\frac{i_e}{k\epsilon^{1.5}} = -\frac{\partial \phi_e}{\partial x} - \frac{2RT}{cF}\left(-t_-^\bullet + \frac{c\hat{V}_o}{2(1 - c\hat{V})}\right)\frac{\partial c}{\partial x} \quad [12]$$

The current in the matrix phase is governed by Ohm's law, given as

$$i_m = -\sigma_{eff}\frac{\partial \phi_m}{\partial x} \quad [13]$$

where

$$\sigma_{eff} = \sigma(1 - \epsilon^o)^{1.5} \quad [14]$$

Also, the matrix phase and solution phase current densities sum to the applied discharge current and are related to the discharge load by

$$i_m + i_e = i_{app} = \frac{E}{R_L A} \quad [15]$$

i_m can be eliminated from Eq. 13 using Eq. 15 to give

$$i_{app} - i_e = -\sigma_{eff}\frac{\partial \phi_m}{\partial x} \quad [16]$$

The six unknown variables in the system of equations are c, ϵ, $v^\bullet$, i_e, ϕ_m, and ϕ_e. The six equations are conservation of current using the Butler-Volmer equation, Eq. 5, the electrolyte balance, Eq. 8; the solid species balance, Eq. 9; overall material balance, Eq. 11, current balance in the electrolyte, Eq. 12; and the current balance in the matrix phase, Eq. 16. The same unknown variables exist in other regions in the cell (separator, LiCl film, and the interfaces) and a similar set of six equations is developed for those various regions, as shown in detail earlier by Evans *et al.*[4]

Cell energy balance.—In this work, the cell is assumed to have a uniform temperature that changes with time. The energy balance follows from the first law of thermodynamics, and the ambient temperature is held constant. This treatment is similar to the work done by Tsaur and Pollard[3] and Evans *et al.*[4] The overall energy balance is given by

$$C_p\frac{dT}{dt} = -h_o(T - T_A) - i_{app}(E_{tn} - E) \quad [17]$$

where E_{tn}, known as the thermoneutral potential, is the theoretical open-circuit potential of the cell at absolute zero. The heat-transfer coefficient (h_o) and the heat capacity (C_p) are based on the surface area of the electrode. Initially, the cell is assumed to be at ambient temperature, and therefore $T = T_A$.

Method of solution.—The system of coupled, nonlinear, partial differential equations describing the Li/$SOCl_2$ cell is solved numerically. The spatial derivatives are approximated using three-point finite differences, and implicit stepping is used for the time derivatives. The resulting set of coupled, nonlinear, algebraic equations is solved using deBoor's banded matrix solver,[13] which employs a Newton-Raphson algorithm. The procedure is iterative and requires initial guesses of the unknowns, which were the converged values of the previous time steps.

Results and Discussion

A complete list of parameters used in the model is given in Table I. Some of these parameters are either available in the literature (*e.g.*, conductivity) or known at the time of cell assembly (*e.g.*, cathode thickness). Although the literature contains conductivity data, it is not available over the entire range of temperature needed nor is it in a form convenient for incorporation into the model. Therefore, correlations are developed in the Appendix for conductivity as a function of concentration and temperature.

The other parameters given in Table I are either not available (*e.g.*, transport and kinetic parameters), change during discharge (*e.g.*, cathode thickness due to swelling), or depend on how the data is collected (*e.g.*, external heat-transfer coefficient). Therefore, the first task was to use the model to estimate all unknown parameters. A sequential approach to the required parameter estimation is described in the following discussion. Although this approach may seem simplistic, the resulting parameter values make physical sense. In addition, the validity of the parameters, and the interactions among them, are tested by comparing entire simulated and experimental discharge curves over the complete operating range of temperature and load. Although refinement in the kinetic parameters is recommended via half-cell experiments, this work is the first attempt to obtain reasonable estimates of kinetic and transport parameters for the Li/$SOCl_2$ system over a wide range of temperatures.

External heat-transfer.—The heat-transfer coefficient was obtained by matching the simulated temperature rise in the cell to the rise in skin temperature observed experimentally. At most temperatures and loads, the temperature rise was small. However, at 25°C and 10 Ω (*i.e.*, a high current), the skin temperature rose by approximately 5°C. Under these operation conditions, the heat-transfer coefficient was adjusted in the model until a temperature rise of 5°C was obtained. The value of the heat-transfer coefficient, $h_o = 6 \times 10^{-4}$ J/cm^2 K, was used for all subsequent simulations. This value is consistent with that used in the earlier model.[4]

Table I. A list of parameters used in the model simulations reported here.

Parameter	Value	Ref.	Parameter	Value	Ref.
$\hat{V}$ (cm^3/mol)	77.97	4, 18	ξ	0.05	4
$\hat{V}_{LiCl}$ (cm^3/mol)	20.5	19	κ (Ω^{-1} cm^{-1})	Eq. A-1	17
$\hat{V}_o$ (cm^3/mol)	72.63	14	D (cm^2/s)	Eq. 21	d
E_{tn} (V)	−3.723	20	ϵ_s	0.95	c
dE_{oc}/dT (V/K)	2.28×10^{-4}	20	ϵ_m^o	0.8	c
$U_{1,ref}$ (V)	$E_{tn} + dE_{oc}/dT$	21	d_s (cm)	0.023	c
$U_{2,ref}$ (V)	0.0	a	d_m^o (cm)	0.07	c
σ (Ω^{-1} cm^{-1})	45.5	22	c_o (mol/cm^3)	0.001	c
C_p (J/cm^2 K)	0.2	3, 4, 10	$i_{o,1,ref}$ (A/cm^2)	Eq. 23	d
h_o (J/cm^2 K s)	6×10^{-4}	4	$a_o i_{o,2,ref}$ (A/cm^3)	Eq. 22	d
Q_{max} (Ah)	16.7	b	$t_+^\bullet$	0.7	d
ϵ_m	0.835	b	$\alpha_{a,1}$	0.8	d
d_m (cm)	0.085	b	$\alpha_{c,2}$	0.3	d
A	180 cm^2	c			

[a] Reference reaction.
[b] Assuming the experimentally observed maximum capacity (16.2 Ah at 25°C and 250 Ω load) represents 97% of the theoretical maximum.
[c] Measured from cell design.
[d] Estimated using the model and experimental data.

S0013-4651(98)07-107-9 CCC: $7.00

Cathode dimension (effect of swelling).—The thickness and porosity of the porous cathode are measured prior to assembly and are listed in Table I as d_m^o and ϵ_m^o, respectively. Due to excess electrolyte in the header of the cell, the battery continues to discharge until the front of the porous cathode becomes plugged with LiCl. Therefore, the maximum capacity of the cell can be calculated based on the volume available for LiCl precipitation. According to reaction 1, Faraday's law gives

$$Q_{max} = \frac{\epsilon_m d_m AF}{\hat{V}_{LiCl}} \quad [18]$$

Using the porosity and thickness values prior to assembly (*i.e.*, d_m^o and ϵ_m^o) the maximum capacity would be 11.3 Ah, while capacities as high as 16.2 Ah were observed experimentally. The extra capacity can be attributed to the increased volume due to cathode swelling.

The extent of cathode swelling can be estimated by assuming the highest capacity obtained experimentally (16.2 Ah at 250 Ω and 25°C) represents about 97% of the theoretical capacity, or Q_{max} = 16.7 Ah. A discharge efficiency of 97% was arrived at by noting that when diffusion and kinetic contributions to the nonuniformity are minimized (*i.e.*, large D and small $i_{o,2,ref}$), ohmic losses lead to a capacity loss of about 2%. Assuming an additional 1% loss due to diffusion and kinetic effects leads to a total efficiency of 97%. Let the average matrix-phase porosity and thickness of the cathode over the course of discharge be ϵ_m and d_m, respectively. Then the additional thickness due to swelling, Δd, affects the matrix-phase thickness and porosity via the following equations

$$d = d_m^o + \Delta d \quad [19]$$

$$\epsilon_m d_m = \epsilon_m^o d_m^o + \Delta d \quad [20]$$

Knowing Q_{max}, ϵ_m^o, and d_m^o, Eq. 18-20 give ϵ_m = 0.835 and d_m = 0.085 cm.

Diffusion coefficient.—The model can be used to obtain the diffusion coefficient, D, as a function of temperature by recognizing that kinetic and mass-transfer resistances increase as the temperature decreases. Since a large kinetic resistance leads to a uniform reaction and a large mass-transfer resistance has the opposite effect, premature plugging of the pores at the front of the electrode at low temperatures is dominated by mass-transfer limitations. As verified later, the simulated capacity was not affected by the $SOCl_2$ kinetics for all loads at −55, −40, and −18°C, and the 10 Ω load at 25°C. Therefore, capacity data at low temperatures can be used to get the diffusion coefficient, D, as a function of temperature and the transference number, $t_+^•$. The transference number was adjusted such that D is relatively insensitive to the loads and $t_+^•$ is insensitive to temperature. A value of $t_+^•$ = 0.7 met this criteria. The transference number is assumed to be insensitive to temperature, which signifies that the temperature dependency of the anion diffusion coefficient is similar to that of the cation.

Fixing $t_+^•$ at 0.7, a diffusion coefficient was obtained that matched the experimental and simulated capacity data at different loads and temperatures. At least three experimental discharge curves were collected at each load and temperature. Therefore, the symbols in Fig. 2 represent the diffusion coefficient obtained from the mean capacity, while the upper and lower limits on the error bars are the diffusion coefficients at the highest and lowest capacity, respectively. The solid line through these data is the following modified Arrhenius expression

$$D = 1.726 \times 10^{16} \exp\left(-\frac{2.315 \times 10^4}{T} + \frac{2.395 \times 10^6}{T^2}\right) \quad [21]$$

where T is in kelvin. Equation 21 is a semi-empirical representation of the diffusion coefficient in Arrhenius form, where the activation energy is temperature dependent. The temperature-dependent activation energy is approximately 2.4 and 14.1 kcal/mol at −55 and 25°C, respectively. Tsaur and Pollard[3] and Evans *et al.*[4] report a constant activation energy of 3.00 and 5.92 kcal/mol, respectively, assuming the same temperature dependence as for the electrolyte conductivity. Equation 21 should be used with caution for temperatures below −55°C, since the diffusion coefficient goes through a minimum (*i.e.*, zero activation energy) at approximately −66°C.

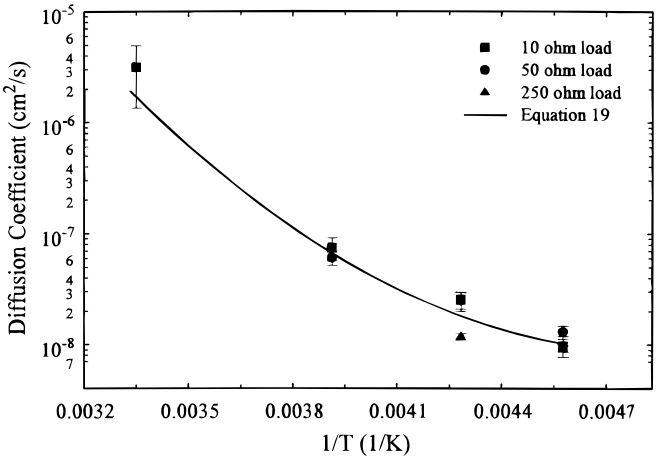

Figure 2. Diffusion coefficient as a function of temperature for varying load. The symbols represent the value of D that results in a fit of the simulated to the experimental capacity. The solid line is the best fit given by Eq. 21.

As stated earlier, the simulated capacity is relatively insensitive to D or $t_+^•$ for temperatures above 25°C. For example, at 25°C a four order-of-magnitude increase in D increases the capacity by only 0.4%. Decreasing D by a factor of 5 or decreasing $t_+^•$ from 0.7 to 0.5 decreases the capacity by 5 and 1%, respectively. In contrast, the capacity at −55°C is very sensitive to D and $t_+^•$. A 9% increase or decrease in D changes the capacity by 5%, and decreasing $t_+^•$ from 0.7 to 0.5 decreases the capacity by a factor of 2. The magnitude of D given in Eq. 21 at 25°C is consistent with the value used previously.[3,4] For example, using Evans *et al.*[4] value for $D = 3.83 \times 10^{-6}$ cm²/s and $t_+^• = 0.5$ gives a capacity at a 50 Ω discharge that is only 0.3% higher than when $D = 1.65 \times 10^{-6}$ from Eq. 21 and $t_+^•$ = 0.7 are used. However, using their D value at −55°C (*i.e.*, $D = 9.19 \times 10^{-6}$ cm²/s and $t_+^• = 0.5$) results in a capacity of 13.9 Ah. The experimental capacity at −55°C and 50 Ω is 4.0 Ah (see Fig. 3 and 5). Since electrolyte transport, not kinetics, determines the capacity under these conditions, the diffusion coefficient must be significantly less than that reported previously.

Kinetics for the main reaction at the cathode.—In contrast to lower temperatures, the discharge capacity at high temperatures is dictated by the kinetics for $SOCl_2$. Facile kinetics yields a nonuniform reaction in porous electrodes[6] which results in premature pore plugging at the front of the electrode. Therefore, the capacity data for all loads at 25 and 49°C was used to estimate the kinetic parameters for $SOCl_2$ reduction, $a^o i_{0,2,ref}$ and $\alpha_{c,2}$ (it is assumed that $\alpha_{c,2} + \alpha_{c,2} = 2$). As with the diffusion coefficient (shown in Fig. 2), $a^o i_{o,2,ref}$ was obtained by fitting the simulated capacity to the experimental capacity. The cathodic transfer coefficient, $\alpha_{c,2}$, was adjusted such that it was insensitive to load and temperature, and $a^o i_{o,2,ref}$ was insensitive to the load. The result is $\alpha_{c,2}$ = 0.3, and a value for $a^o i_{o,2,ref}$ at the two temperatures. The $a^o i_{o,2,ref}$ values at these two temperatures were fit to an Arrhenius expression to give

$$a^o i_{o,2,ref} = 2.5 \times 10^6 \exp\left(-\frac{5500}{T}\right) \quad [22]$$

where T is in kelvin. The activation energy for $SOCl_2$ reduction from Eq. 22 is 10.9 kcal/mol.

As seen in Fig. 5, the capacity is within 85% of the observed maximum capacity of 16.2 Ah at 25 and 49°C. Therefore, decreasing the exchange current density at the cathode has little effect on the predicted capacity. Increasing $a^o i_{o,2,ref}$, however, does affect the capaci-

S0013-4651(98)07-107-9 CCC: $7.00

ty. For example, at 25 and 49°C, the capacity decreases by 5% for a 3.9- and 1.7-fold increase in $a^{o}i_{o,2,ref}$, respectively. The corresponding change in cell voltage is a 1.0 and 0.1% increase, respectively.

Kinetics for the main reaction at the anode.—The kinetic expression for lithium oxidation at the anode is given by[3]

$$i_{app} = i_{o,1,ref}\left[\exp\left(\frac{\alpha_{a,1}F}{RT}\eta_1\right) - \left(\frac{c}{c_{ref}}\right)\exp\left(-\frac{\alpha_{c,1}F}{RT}\eta_1\right)\right] \quad [23]$$

where

$$\eta_1 = \phi_m - \phi_e - U_{1,ref} \quad [24]$$

Once the $SOCl_2$ reduction kinetics and the electrolyte diffusion coefficient are known, the only unknown is Li oxidation kinetics. Li oxidation does not affect the cell capacity,[4] but it does affect the cell voltage. The difference in the cell potential and the open-circuit potential is due to the kinetic loss at the anode, ohmic loss in the separator, and kinetic loss in the porous cathode. The losses through the separator and the porous cathode were calculated using the known conductivity and $SOCl_2$ reduction kinetic parameters. These two losses accounted for the entire voltage loss at high temperature and high load (*i.e.,* low current). Therefore, the loss due to Li oxidation at the anode was negligible except at low temperature and low loads. Using the calculated overpotential at −18, −40, and −55°C for loads of 10 and 50 Ω, a transfer coefficient, α_a, of 0.8 was obtained that made the exchange current density insensitive to the load at low temperatures. The temperature dependence of the exchange current density, $i_{0,1,ref}$, is given as

$$i_{o,1,ref} = 1.157 \times 10^3 \exp\left(-\frac{4641}{T}\right) \quad [25]$$

where T is in kelvin. The activation energy for $i_{0,1,ref}$ as given in Eq. 25 is 9.22 kcal/mol.

The relatively facile kinetics at the anode (*i.e.,* large $i_{0,1,ref}$ values in Eq. 25) mean that the simulated cell voltage is not very sensitive to $i_{0,1,ref}$. For example, an order-of-magnitude change in $i_{0,1,ref}$ at −55°C changes the cell voltage by less than 60 mV (a 2% change). At higher temperatures the change is even less. As stated earlier, the capacity is not affected by the kinetics at the anode.

Comparison of experimental data and model simulations.—Although the parameters are obtained sequentially, the interactions between the various phenomena such as mass-transfer and kinetics have to be captured in order to predict the cell performance with accuracy. The validity of these interactions and the parameters given in Table I are tested by simulating the entire discharge curves and comparing them to the experimental discharge curves. Figure 3 shows the comparison of the simulated discharge curves with the experimental discharge data obtained at −55, −18, and 25°C for 50 Ω load. Figure 4 shows the comparison at −18°C for loads of 10, 50, and 250 Ω. Overall, a very good agreement is observed between the experimental and simulated discharge curves over the entire range of temperature and loads.

In Fig. 5 and 6, the experimental capacity and average cell voltage, respectively, are compared to the simulated values over the entire range of temperature and load. Again, the symbols represent the mean of at least three experimental values, while the error-bar limits represent the high and low values. The cutoff voltage used for the capacity shown in Fig. 5 was 2.0 V for both the experimental and simulated data. The low capacity at lower temperatures is due to mass-transfer limitations in the cathode, while the slight drop in capacity at higher temperatures and lower loads (higher currents) is due to the nonuniform reaction caused by facile kinetics in the cathode. Good agreement between simulated and experimental capacity over the entire range of temperature and load is obtained, with a major exception at −40°C. As seen in Fig. 2, no single value of D could be estimated that would fit the experimental capacity at −40°C for both loads (50 and 250 Ω). Capacity data for more loads at −40°C might be useful in providing more confidence in the estimated diffusion coefficient.

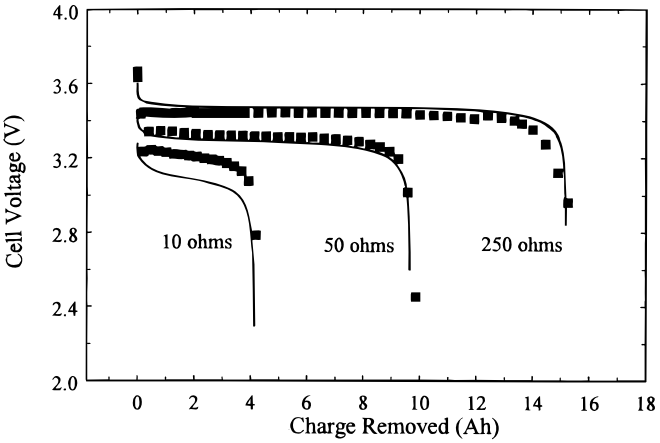

Figure 4. Comparison of experimental and simulated discharge curves at −18°C for loads of 10, 50, and 250 Ω. The symbols represent the experimental data while the solid lines are for the model simulations.

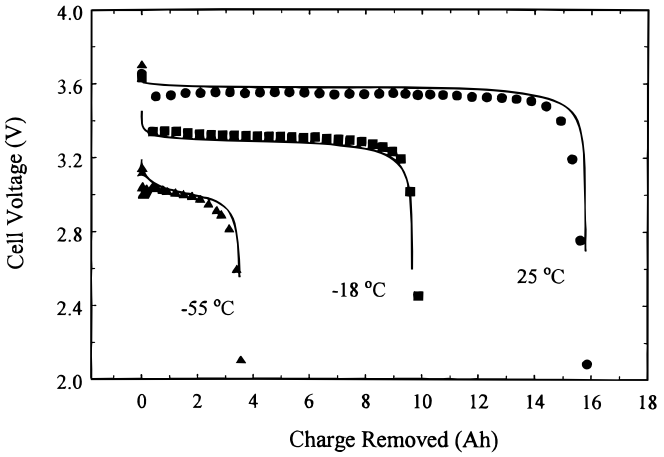

Figure 3. Comparison of experimental and simulated discharge curves for a 50 Ω load at −55, −18, and 25°C. The symbols represent the experimental data while the solid lines are for the model simulations.

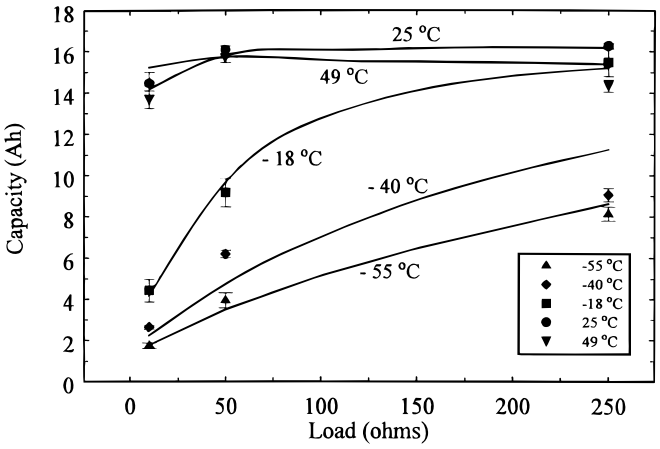

Figure 5. Comparison of the simulated and experimental cell capacity as a function of the load over a temperature range of −55 to 49°C. The solid lines represent the simulated cell capacity and the symbols are the experimental data.

S0013-4651(98)07-107-9 CCC: $7.00

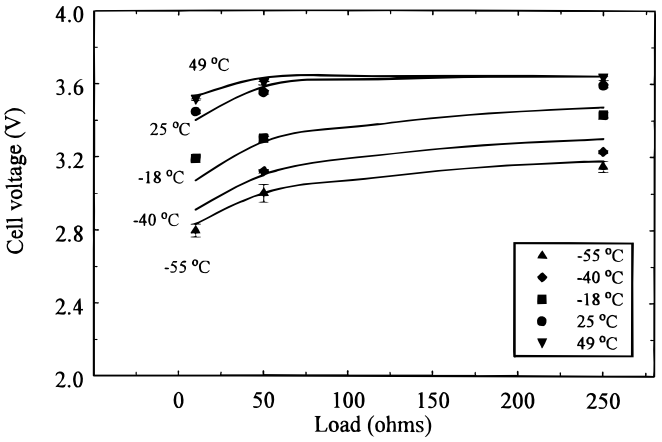

Figure 6. Comparison of the simulated and experimental cell voltage at half the capacity as a function of discharge load over a temperature range of −55 to 49°C. The solid lines represent the simulated cell voltage and the symbols are the experimental data.

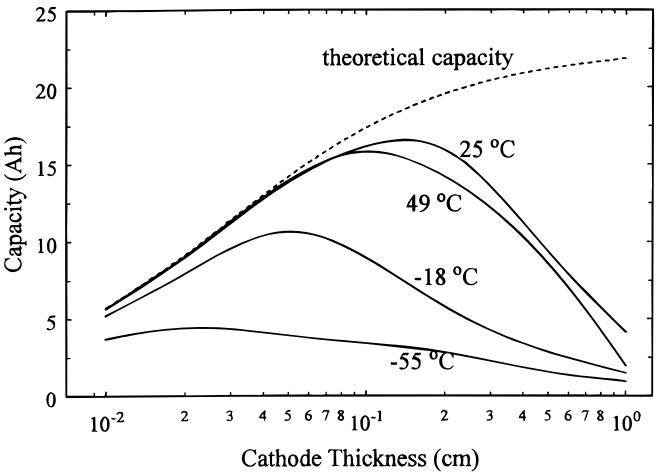

Figure 7. Effect of cathode thickness on the cell capacity for various temperatures at a constant load of 50 Ω. The theoretical capacity (-----) is also shown for a D-size cell as a function of cathode thickness.

The comparison of the experimental and simulated cell voltage shown in Fig. 6 is for the cell voltage at half the capacity delivered. The capacity that was delivered at a cutoff voltage of 2.0 V was noted, and the simulated and experimental cell voltage at half that capacity were compared. As evident from the figure, the simulated cell voltage fits the experimentally obtained values fairly well over the entire range of temperature and load.

Cathode thickness optimization.—With a reliable set of parameters, the model can be used to perform design studies. For example, Fig. 7 and 8 show the effect of cathode thickness on the cell capacity for various temperatures and loads, respectively. For the results shown in Fig. 7 and 8, the following three parameters were held constant at the value of the experimental cells: (*i*) the ratio of the anode capacity to cathode capacity; (*ii*) the ratio of anode area to the cathode; and (*iii*) separator thickness. The solid lines show the predicted capacities from the model and the dashed line is the theoretical capacity for a given thickness. The theoretical capacity, Q_{max}, is obtained when all the pores in the cathode are uniformly filled with LiCl precipitate and is given by Eq. 18 for a cathode-limited design [*i.e.,* the capacity in the anode (Li foil) is more than the cathode]. The theoretical capacity is directly proportional to the volume of the cathode (Ad_m), and it is also dependent on the volume of other components in the cell (two separators and an anode) since the total volume of the cell is a constant. The separators constitute most of the cell volume for thin cathodes and so the theoretical cell capacity is low. As the cathode thickness increases, the theoretical capacity increases because the separator accounts for proportionately less of the cell volume. The theoretical capacity of the cell eventually levels off as cathode active material becomes essentially all cell volume.

In Fig. 7, the ohmic, kinetic, or mass-transfer limitations do not arise in the thin cathodes at high temperatures, and this leads to capacities close to theoretical maximum. However, ohmic and mass-transfer limitations at lower temperatures lead to lower than theoretical capacities. As the cathode's thickness increases, its area decreases since the total volume is conserved. This results in an increase in current density for the same load and therefore, a less uniform reaction. The mass-transfer limitations are insignificant at higher temperatures, but the facile kinetics lead to nonuniformity in the reaction in the porous electrode. For example, at cathode thickness greater than 1 mm, the reaction is more nonuniform at 49°C compared to 25°C, resulting in lower capacity. There exists an optimum thickness at a given load and temperature when the cell capacity is a maximum. For the D-size cell shown here, a cathode thickness of approximately 0.15 cm at 25°C and 50 Ω load would result in maximum capacity.

In Fig. 8 the theoretical capacity is obtained for very low currents (*i.e.,* high loads) when there are no ohmic, kinetic, or diffusional limitations. Although the predicted capacity at 50 and 250 Ω is not very different, the kinetic limitations are high enough to lead to nonuniformity for a thicker electrode, resulting in less than theoretical capacity. The lower capacity at 10 Ω load is due to the nonuniformity that arises due to a combination of both the $SOCl_2$ reduction kinetics and mass transfer.

Conclusions

A one-dimensional mathematical model for the Li/$SOCl_2$ primary battery was developed and used for parameter estimation and design studies. The model formulation is based on the fundamental conservation laws using porous electrode theory and concentrated solution theory. The model was used to estimate the transference number, the diffusion coefficient, and the kinetic parameters for the reactions at the anode and the cathode as a function of temperature. These parameters were obtained by fitting the simulated capacity and average cell voltage to the experimental capacity and average cell voltage, respectively, over a wide range of temperatures (−55 to 49°C) and discharge loads (10 to 250 Ω). The experiments were performed on D-sized, cathode-limited, spirally wound cells. Although refinement in the kinetic parameters is recommended via half-cell experiments, this work is the first attempt to obtain reasonable estimates of kinetic and transport parameters for the Li/$SOCl_2$ system over a wide range of temperatures. The results from the model indicate that the cell capacity is governed by the material transport at

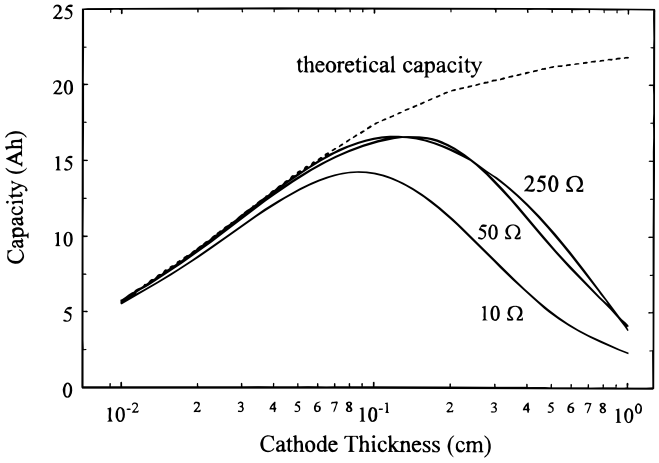

Figure 8. Effect of cathode thickness on cell capacity for constant load discharge for various loads at 25°C. The theoretical capacity (-----) is also shown for a D-size cell as a function of cathode thickness.

S0013-4651(98)07-107-9 CCC: $7.00

lower temperatures, while the $SOCl_2$ reduction kinetics controls the capacity at higher temperatures (25°C and above). Finally, the model was used to study the effect of cathode thickness on the cell capacity as a function of load and temperature. An optimum thickness exists depending on the load and temperature in order to deliver maximum capacity.

Acknowledgments

The authors acknowledge the financial support of Sandia National Laboratories. Sandia is a multiprogram laboratory operated by Sandia Corporation, a Lockheed Martin Company, for the United States Department of Energy under contract no. DE-AC04-94AL85000. Experimental measurements of cell capacity and voltage were conducted by H. L. Case at Sandia National Laboratories.

The University of South Carolina assisted in meeting the publication costs of this article.

Appendix

Conductivity

The conductivity of the Li/$SOCl_2$ electrolyte solution is a strong function of temperature and the salt ($LiAlCl_4$) concentration.[14,15] Correlations have been developed to evaluate the conductivity for a given temperature and concentration.[3,4] These correlations fit the data well at 25°C, up to a salt concentration of 2 M, but do not match the conductivity at other temperatures and/or higher concentrations. The specific conductivity of the electrolyte solution initially increases with increasing salt concentration, up to a concentration of 1.8 M. Since the existing correlations were obtained using experimental data over a concentration range of 0.000313-2.0 M, the conductivity was assumed to be constant above 2.0 M in the available correlations. However, the conductivity actually decreases almost linearly after reaching the maximum.[16] Berg *et al.*[17] measured the specific conductivity of the system as a function of temperature (−20 to 70°C) and composition, shown as the symbols in Fig. A-1. Since the concentration is an unknown function of temperature, measuring the specific conductivity as a function of temperature and concentration is not adequate unless the solution is prepared at the temperature in question or a correction procedure is applied. Therefore, Berg *et al.*[17] reported the specific conductivity as a function of the mole fraction of $LiAlCl_4$, instead of the concentration of $LiAlCl_4$ in $SOCl_2$ as a function of temperature, and also reported the corresponding concentration at that temperature. Since the present model is in terms of concentration, the data from Berg *et al.*[17] was used to correlate the specific conductivity to the concentration and temperature, and it was found that the activation energy for the conductivity is a linear function of the concentration over the reported temperature range (−20 to 70°C). The specific conductivity can be expressed as

$$\kappa = \begin{cases} 9.79c\ \exp(2039.09c - 2.5055 \times 10^5 c^2)\ \exp\left[-\dfrac{(4.88 \times 10^5 c - 71.73)}{T}\right] & (c < 1.8\ \text{M}) \\ 1.6 \times 10^{-2}\ \exp(1.63 \times 10^3 c)\exp\left[-\dfrac{(4.88 \times 10^5 c - 71.73)}{T}\right] & (1.8\ \text{M} \le c < 2.0\ \text{M}) \\ (2.11 \times 10^{-2} - 2.53c)\ \exp(1.63 \times 10^3 c)\ \exp\left[-\dfrac{(4.88 \times 10^5 c - 71.73)}{T}\right] & (c \ge 2.0\ \text{M}) \end{cases}$$

Figure A-1 shows the comparison of experimental data and the conductivities obtained using this expressions over the reported temperature range (−20 to 45°C). Though this expression was obtained using the reported temperature range, it was used in the model for the entire temperature range (−55 to 49°C) due to lack of additional data.

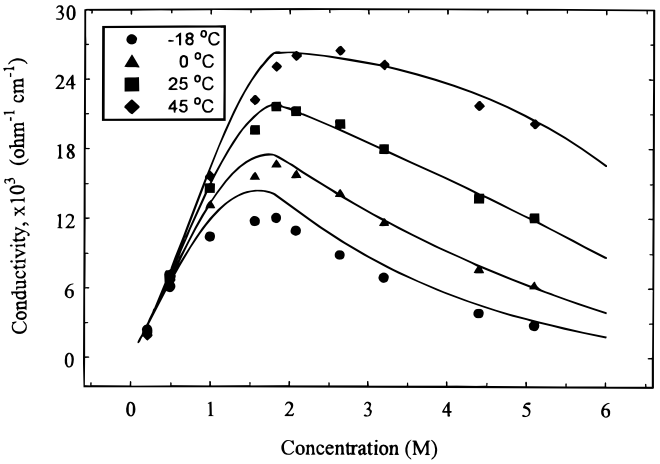

Figure A-1. Specific conductivity for the $SOCl_2$-$LiAlCl_4$ system over a temperature range of −18 to 45°C. The symbols represent the data from Ref. 18, and the lines represent the specific conductivity as obtained using the expression in the Appendix.

List of Symbols

a	specific surface area of the porous cathode, cm^{-1}
A	cross-sectional area of the porous cathode, cm^2
C_p	heat capacity of cell, J/cm^2 K
c	electrolyte salt concentration, mol/cm^3
c_i	concentration of species i, mol/cm^3
D	diffusion coefficient of the binary electrolyte, cm^2/s
d_m	thickness of cathode, cm
d_m^o	thickness of cathode prior to assembly, cm
E	cell voltage, V
E_{tn}	thermoneutral potential, V
E_{oc}	open-circuit potential, V
F	Faraday's constant, 96487 C/mol
h_o	heat-transfer coefficient, J/cm^2 K s
$i_{o,k,ref}$	exchange current density of reaction k at c_{ref}, A/cm^2
i	superficial current density, A/cm^2
j_2	reaction current per unit volume due to $SOCl_2$ reduction, A/cm^3
Q_{max}	maximum capacity of the cell, C
R	universal gas constant, 8.314 J/mol K
R_L	discharge load, Ω
$t_i^\bullet$	transference number of species i relative to $v^\bullet$
T	cell temperature, K
T_A	ambient temperature, K
t	time, s
$U_{k,ref}$	potential of reaction k relative to the reference electrode, V
$v^\bullet$	superficial volume average velocity, cm/s
$\hat{V}$	partial molar volume of electrolyte salt, cm^3/mol
$\hat{V}_i$	partial molar volume of species i, cm^3/mol
x	direction normal to current collector, cm
z_i	charge number of species i

Greek

$\alpha_{a,k}$	transfer coefficient in the anodic direction of reaction k
$\alpha_{c,k}$	transfer coefficient in the cathodic direction of reaction k
Δd	change in cathode thickness
ϵ	porosity
κ	electrolyte conductivity, Ω^{-1} cm^{-1}
ξ	morphology parameter
σ	conductivity of the matrix phase, Ω^{-1} cm^{-1}
ϕ	potential, V

Subscripts

app	applied
e	electrolyte phase
eff	effective
i	species i
LiCl	lithium chloride precipitate
m	solid matrix phase
o	solvent
s	separator

S0013-4651(98)07-107-9 CCC: $7.00

+	cation
−	anion

Superscripts

o	initial

References

1. D. H. Johnson, A. D. Ayers, R. L. Zupancic, V. S. Alberto, and J. C. Bailey, *J. Power Sources*, **2,** 61 (1984).
2. S. Surampandi, G. Halpert, and I. Stien, JPL Publication 86-15 (June 1986).
3. K. Tsaur and R. Pollard, *J. Electrochem. Soc.*, **131,** 975 (1984).
4. T. I. Evans, T. V. Nguyen, and R. E. White, *J. Electrochem. Soc.*, **136,** 328 (1986).
5. J. Newman and W. Tiedemann, *AIChE. J.*, **21,** 25 (1975).
6. J. Newman, *Electrochemical Systems*, Prentice Hall, Inc., Englewood Cliffs, NJ (1973).
7. T. I. Evans and R. E. White, *J. Electrochem. Soc.*, **136,** 2798 (1989).
8. M. Jain and J. W. Weidner, *J. Electrochem. Soc.*, **146,** 1370 (1999).
9. Y. I. Cho, *J. Electrochem. Soc.*, **134,** 771 (1987).
10. T. I. Evans and R. E. White, *J. Electrochem. Soc.*, **136,** 2145 (1989).
11. N. Marincic, *J. Appl. Electrochem.*, **5,** 313 (1975).
12. J. S. Dunning, D. N. Bennion, and J. Newman, *J. Electrochem. Soc.*, **120,** 906 (1973).
13. C. DeBoor, *A Practical Guide to Splines*, Springer-Verlag, New York (1978).
14. S. Szpak and H. V. Venkatasetty, *J. Electrochem. Soc.*, **131,** 961 (1984).
15. H. V. Venkatasetty and D. J. Saathoff, *J. Electrochem. Soc.*, **128,** 773 (1981).
16. A. N. Dey and J. Miller, *J. Electrochem. Soc.*, **126,** 1445 (1979).
17. R. W. Berg, H. A. Hjuler, A. P. L. Sondergaard, and N. J. Bjerrum, *J. Electrochem. Soc.*, **136,** 323 (1989).
18. W. K. Behl, J. A. Christopulos, M. Ramirez, and S. Gilman, *J. Electrochem. Soc.*, **120,** 1619 (1973).
19. R. H. Perry and D. Green, *Chemical Engineers, Handbook*, 6th ed., McGraw-Hill, New York (1984).
20. N. A. Godshall and J. R. Driscoll, *J. Electrochem. Soc.*, **126,** 1445 (1979).
21. N. A. Godshall and J. R. Driscoll, *J. Electrochem. Soc.*, **131,** 2221 (1984).
22. A. N. Dey, *J. Electrochem. Soc.*, **126,** 2052 (1979).